Met. Mater. Int., Vol. 21, No. 3 (2015), pp. 453~460
doi: 10.1007/s12540-015-4397-7

Ambient and Cryogenic S-N Fatigue Behavior of Fe15Mn Steel and Its Weld

Daeho Jeong[1], Taedong Park[2], Jongsub Lee[3], and Sangshik Kim[1,*]

[1]Department of Mat. Sci. and Eng., ReCAPT, Gyeongsang National University, Chinju 660-701, Korea
[2]Industrial Technical Institute, Hyundai Heavy Industries, Ulsan 682-792, Korea
[3]Technical Research Laboratory, POSCO, Pohang 790-785, Korea

(received date: 23 August 2014 / accepted date: 4 November 2014)

The S-N fatigue behavior of Fe15Mn (Fe-0.7C-15Mn-2Al) austenitic steel, including base metal and butt-welded joint, was investigated at 298 K and 110 K, and the results were compared to those of STS304L (Fe-1Si-2Mn-20Cr-10Ni) counterparts. Both specimens showed improved resistance to S-N fatigue with decreasing temperature from 298 K to 110 K. The resistance to S-N fatigue of Fe15Mn steel was greater at 298 K, while it was lower at 110 K, than STS304L steel. Unlike STS304L, Fe15Mn steel did not show any notable transformation induced plasticity and twining-induced plasticity effect under fatigue loading at ambient and cryogenic temperatures. The S-N fatigue behavior of Fe15Mn steel was strongly dependent on tensile strength at both ambient and cryogenic temperatures. Similar S-N fatigue behavior was also observed for the butt-welded joints of Fe15Mn steel. The S-N fatigue behavior of Fe15Mn steel and its weld was discussed based on the fractographic and microscopic observations.

Keywords: fatigue, welding, twinning, high manganese steel, cryogenic temperature

1. INTRODUCTION

Extensive research works have been conducted to develop high manganese (Mn) austenitic steels with excellent strength-ductility combination at ambient and cryogenic temperatures, utilizing transformation induced plasticity (TRIP) and twining-induced plasticity (TWIP) effect [1-3]. The steels with Mn contents ranging from 15 to 30 wt% are under consideration for the application in a variety of fields, such as the material for LNG liquified natural gas (LNG) tankage [5-8] and cryogenic pipelines in offshore industry [4]. While the plastic deformation of high Mn steel is mostly accommodated by the slip mechanism, TRIP/TWIP effect can also contribute the deformation [9,10]. The TRIP/TWIP effect during deformation is largely correlated to the stacking fault energy (SFE) in the austenitic matrix [11], which is mainly determined by chemical composition and thermo-mechanical treatment [12-14]. Lowering SFE promotes the slip planarity and reduces the propensity of cross slip [15-19]. Typically, TRIP steels exhibit a very low SFE, while TWIP steels are characterized by higher SFE, and high Mn steels with medium SFE values may show both effects [15,20,21]. It has been reported that twinning occurred in stable austenite matrix with the SFE value of about 25 mJ/m^2 [20,22,23], while dislocation glide was triggered at higher SFE values of over 60 mJ/m^2 [22,24]. Allain *et al*. [25] have reported that duplicative transformations of TRIP and TWIP can occur in the Fe-Mn-C system with the SFE value lower than 18 mJ/m^2, while the mechanical twinning takes place for the SFE values ranging between 12 and 35 mJ/m^2.

For the recently developed high strength, high Mn steels featuring TRIP and/or TWIP effect, the knowledge on fatigue is extremely limited. Particularly for the TWIP steel, there are currently only two papers that report on the fatigue properties in low- [26] and high-cycle fatigue regimes [27]. In both cases, it has been found that no new mechanical twins are formed under cyclic loading of smooth specimens. It is still controversial why TWIP steels display mechanical twins under monotonic tensile straining already after a strain of 2%, but no mechanical twins are formed in the course of cyclic deformation. This seems to be true even at low-cycle fatigue regime, e.g. in the instance that the total strain amplitude was 0.6% [28]. The initiation of mechanical twins requires a critical dislocation density [29], and El-Danaf *et al*. [30] proposed a criterion for twinning in low-SFE FCC metals. They have argued that the formation of mechanical twins necessitates that the dislocation slip is homogenous with length scale close to the initial grain size. The combination of high dislocation density and a large homogenous deformation length scale in the deformed low-SFE metals would therefore promote the initiation of mechanical twins [27]. Under cyclic straining, however, the deformation is inhomogeneous, as indicated by the formation of local intense slip bands where plasticity is strongly localized [31].

*Corresponding author: sang@gnu.ac.kr

In TRIP steels, strain-induced martensite can form in monotonic straining [22]. For example, the strain induced martensite can be formed in monotonic deformation of metastable austenitic stainless steels, the amount of which depends on the stability of steel, deformation temperature and strain [32]. However, no strain-induced martensite has been detected on the fatigued high Mn steels in microscopic examination. Baudry and Pineau [33] have proposed that critical plastic strain amplitude that varies with different chemical composition and temperature is required beyond which strain-induced martensite can form. The amount of strain-induced martensite tends to increase with increasing number of cycles (i.e., accumulated strain).

In this study, the S-N fatigue behavior of Fe15Mn steel and its weld was investigated at ambient and cryogenic temperatures and the results were compared to that of STS304L. The S-N fatigue tests were conducted at an R ratio of 0.1 under a uniaxial loading condition at 298 K and 110 K, respectively. The fracture surface of fatigue initiation area of S-N fatigue tested specimens was examined by using a scanning electron microscope (SEM). The S-N fatigue behavior of high Mn austenitic steel was discussed based on the microstructural and the fractographic observation.

2. EXPERIMENTAL PROCEDURES

The S-N fatigue tests were conducted on 3 mm thick Fe15Mn steel (supplied by POSCO, Korea) and STS304L stainless steel as a reference, in their as-received forms and butt-welded joints by GTAW process. Table 1 shows the specimen designation and the chemical composition of each specimen. For the micrographic observation, each specimen was polished and etched by using a 2% nital solution for 20~50 seconds. The round bar specimens for the tensile tests and flat hourglass typed specimens for the S-N fatigue tests were prepared from both as-received sheet and butt-welded joint. The schematic illustration of (a) tensile and (b) fatigue specimen

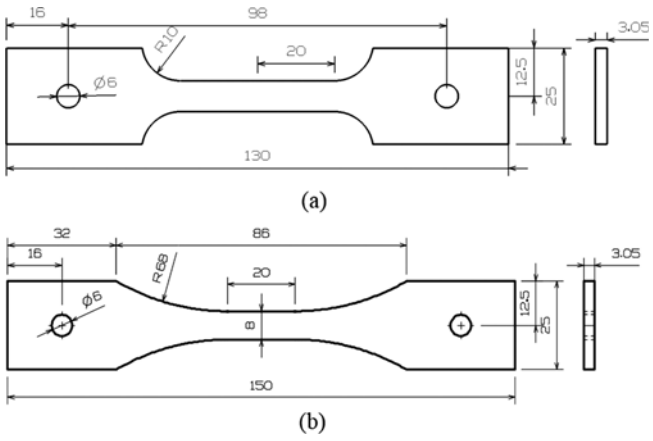

Fig. 1. The schematic illustration of (a) tensile and (b) fatigue specimens used in this study. All the units are mm.

is shown in Fig. 1. The tensile tests were conducted on the base metal (BM) and the welded joints at a nominal strain rate of 10^{-3}/sec at 298 K and 110 K. The tensile properties of Fe15Mn and STS304L, both BM and weld, at 298 K and 110 K are summarized in Table 2. The S-N fatigue tests were conducted on a servo-hydraulic testing machine (Instron Model 8516) at an R ratio of 0.1 under a uniaxial loading condition with a sinusoidal frequency of 30 Hz at 298 K and 110 K, respectively, in accordance with ASTM E466 [34]. The run-out fatigue specimens were defined as those not failed up to 2×10^6 cycles. An environmental chamber was utilized to maintain the testing temperature of 110 K which is the temperature of LNG. In order to identify the possible TWIP effect, the Fe15Mn specimens were fatigued at 298 K and 110 K with the maximum applied stress of 750 MPa, the tests were intermittently stopped every 10,000 cycles, and the surface was observed after polishing using an optical microscope. For the observation of mechanical twinning, selected specimens were color-tint etched using a solution of 2% nital and 20% aqueous $Na_2S_2O_5$ [35], and the optical microscopy and the EBSD techniqued

Table 1. The chemical composition of Fe15Mn and STS304L specimens

Material	C	Si	Mn	Al	P	S	Cr	Ni	N	Fe
Fe15Mn	0.69		15.5	2					0.004	Bal.
STS304L	0.03	1	2		0.045	0.03	18 ~ 20	8 ~12		Bal.

Table 2. The tensile properties of Fe15Mn and STS304L, both base metal and butt-welded joint, at 298 K and 110 K

Material	Temp. (K)	Yield strength (MPa)	Tensile strength (MPa)	Tensile elongation (%)
Fe15Mn	298	494	951	72
	110	827	1,251	25
STS304L	298	299	733	63
	110	313	1,493	32
Fe15Mn/Fe15Mn	298	360	696	23
	110	562	837	8
STS304L/STS304L	298	326	613	37
	110	320	1,276	27

were utilized. The amount of martensite possibly formed from austenite was measured using a ferritescope (Fischer model MP30E-S) with the detection resolution of ±1% before and after the tests, both fatigue and tensile, for some selected specimens. Scanning electron microscope (SEM) analysis was conducted on the S-N fatigue tested specimens to examine the fracture mode.

3. RESULTS AND DISCUSSION

Figure 2 shows the optical micrographs of (a) Fe15Mn and (b) STS304L. The austenite single phase and annealing twin bands within the grains were observed for Fe15Mn and STS304L specimens. The average grain size was similar for both specimens ranging from 16 to 18 μm. As shown in Table 2, the Fe15Mn steel has an excellent combination of strength and ductility at ambient and cryogenic temperatures. At room temperature, yield strength (YS), tensile strength (TS) and tensile elongation (TE) were substantially higher for the Fe15Mn specimen than the STS304L specimen. With decreasing temperature from 298 K to 110 K, the Fe15Mn specimens showed a 67% increase in YS and a 32% increase in TS. At 110 K, both specimens showed substantial amount of strain hardening, particularly for the STS304L specimen at 110 K. As a result of this, the TS of STS304L specimen became greater, while the YS was still lower, than that of Fe15Mn at 110 K. The TE was slightly higher for Fe15Mn than STS304L at 298 K, whereas the trend was reversed at 110 K. Figure 3 shows the SEM fractographs of tensile fractured Fe15Mn at (a) 298 K and (b) 110 K. The dimpled rupture mode at 298 K

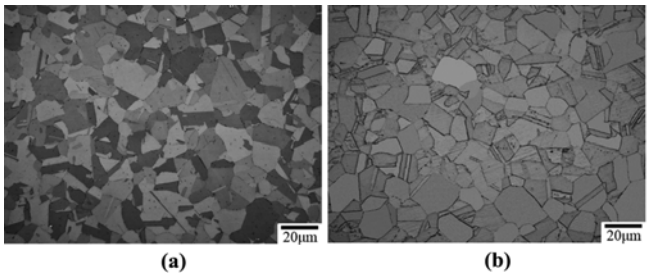

Fig. 2. The optical micrographs of (a) Fe15Mn and (b) STS304L specimens.

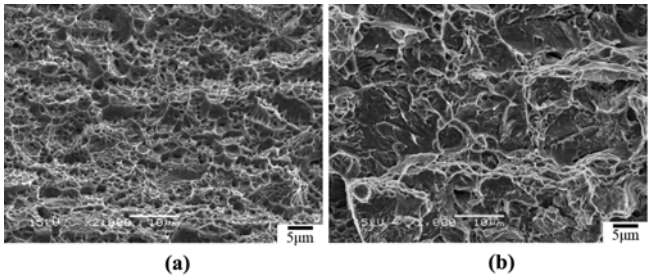

Fig. 3. The SEM fractographs of tensile fractured Fe15Mn specimen at (a) 298 K and (b) 110 K.

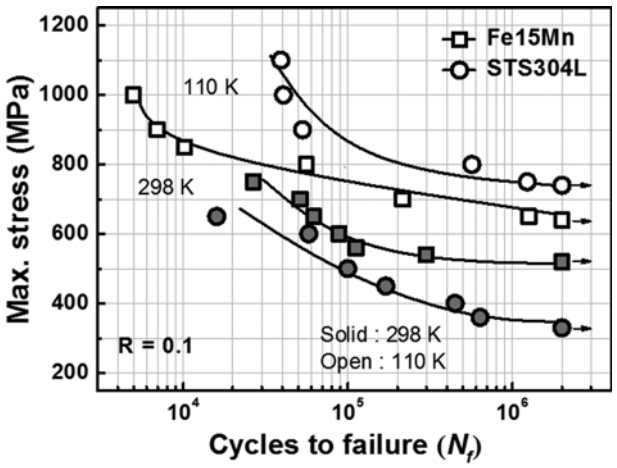

Fig. 4. The S-N fatigue curves of Fe15Mn and STS304L specimens, uni-axially fatigued at 298 K and 110 K.

changed to cleavage with intermittent dimples at 110 K, reflecting a reduced plasticity with decreasing temperature.

Figure 4 shows the S-N fatigue curves of Fe15Mn specimen at 298 K and 110 K, uni-axially fatigued at an R ratio of 0.1. As a reference material, those of commercially available STS304L are also included in this figure. At room temperature, the resistance to S-N fatigue was greater for the Fe15Mn specimen than that for the STS304L specimen. At 110 K, on the other hand, the resistance to S-N fatigue for the Fe15Mn specimen was lower than the STS304L specimen. It was particularly substantial in high applied stress range, and the STS304L specimen showed an abrupt increase in the slope of S-N fatigue curve above the maximum stress of 900 MPa at 110 K. It is generally believed that the resistance to S-N fatigue is largely related to the strength of material, since the slip deformation is prerequisite for the damage accumulation of fatigue [36,37]. It is also noted in Table 2 that the change in S-N fatigue behavior of Fe15Mn and STS304L is closely related to the change in tensile properties with decreasing temperature from 298 K and 110 K. It is, however, still controversial whether the resistance to S-N fatigue is related to the yield strength or the tensile strength. To identify this notion, the S-N fatigue curve of each specimen was normalized by (a) YS and (b) TS in Fig. 5. The fatigue curves normalized by YS values (Fig. 5(a)) showed a substantial scatter with different testing conditions, suggesting that YS values were not appropriate to describe the room and cryogenic S-N fatigue behavior of these alloys. For the S-N fatigue curves normalized by TS values (Fig. 5(b)), on the other hand, four different S-N fatigue lines tended to merge into a single line. It is a strong indication that the fatigue behavior of these alloys is largely dependent on TS, rather than YS. The YS represents the resistance to slip deformation, occurring over a certain range of stress level rather than at a single stress level. It is therefore not appropriate to explain the S-N fatigue behavior of Fe15Mn and STS304L

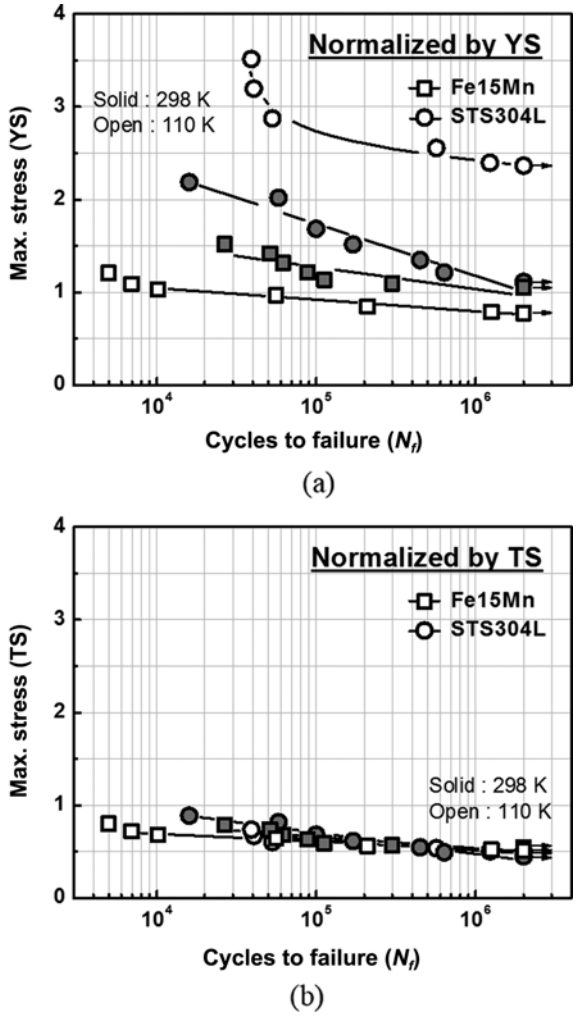

Fig. 5. The S-N fatigue curves of Fe15Mn and STS304L specimens normalized by (a) YS and (b) TS.

specimens, both of which show substantial amount of strain hardening, by YS alone. This is also true for metastable STS304L steels with a considerable amount of strain-induced martensitic transformation during fatigue loading at low temperatures. The S-N fatigue curves normalized by TS values in Fig. 5(b) show that the increase in TS value can explain the abrupt increase in the slope of S-N fatigue diagram of STS304L in high applied stress range at 110 K. It has been well established that the strain-induced martensitic transformation particularly at low temperatures enhances the resistance to S-N fatigue of austenitic stainless steels by increasing the strength of material retarding crack initiation and by inducing compressive residual stress retarding crack propagation [2,38,39]. The greater resistance to S-N fatigue of STS304L at 110 K particularly in high applies stress range is mostly due to the strain-induced martensitic transformation [40].

Figure 6 shows the volume fraction of martensite formed during fatigue loading on Fe15Mn and STS304L specimens

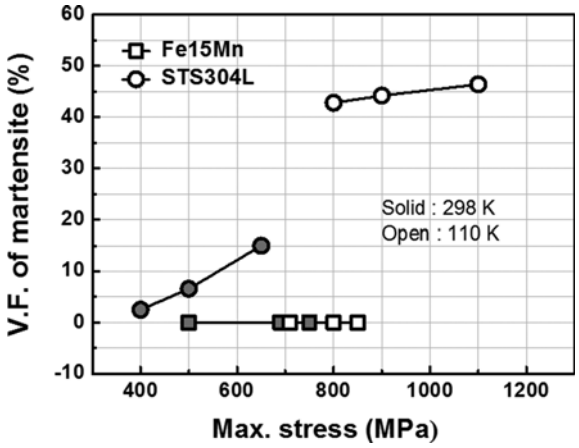

Fig. 6. The volume fraction of martensite formed during fatigue loading on Fe15Mn and STS304L specimens at 298 K and 110 K.

at 298 K and 110 K. It was noted that considerable amount of martensite was formed on the STS304L specimen during fatigue loading, which was dependent on the testing temperature and the applied stress. Approximately 45% of transformed martensite was observed at 110 K, while it was below 15% at 298 K, for the fatigued STS304L specimens. Unlike the STS304L specimen, no notable amount of transformed martensite was measured on the fatigued Fe15Mn specimen. As mentioned previously, the TRIP/TWIP effect is strongly dependent on the SFE of material. The TRIP effect, for example, has been reported to be dominant for the material with the SFE value lower than 18 mJ/m^2, while the mechanical twinning may be encouraged for the SFE values ranging from 12 to 35 mJ/m^2 [25,41]. The predicted SFE for the Fe15Mn specimen was approximately 26 mJ/m^2 [21,42], and the TRIP

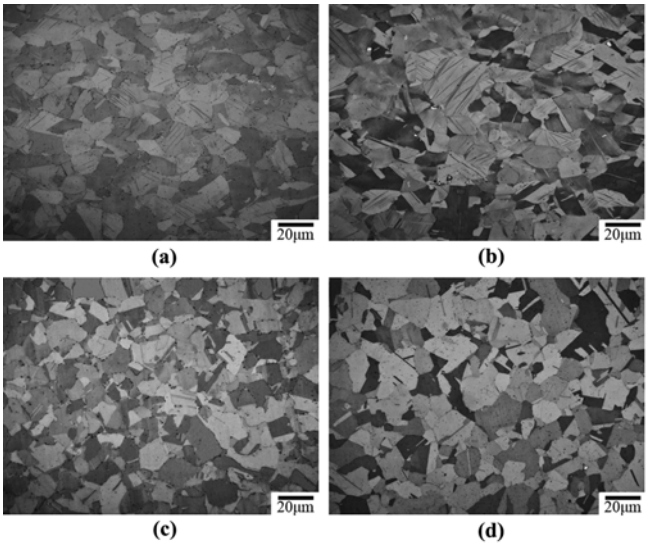

Fig. 7. The optical micrographs of Fe15Mn specimen fatigued at (a) 298 K/10,000 cycles, (b) 298 K/20,000 cycles, (c) 110 K/10,000 cycles, and (d) 110 K/20,000 cycles.

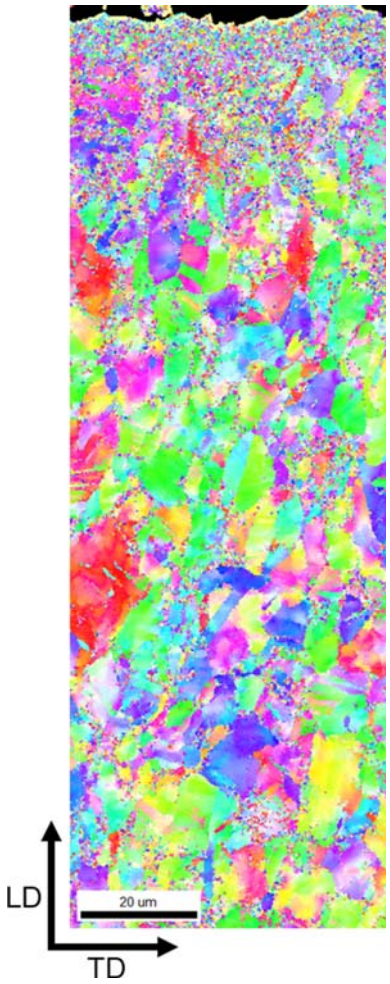

Fig. 8. The EBSD image of fatigue-failed Fe15Mn specimen at 298 K/700 MPa for 51,300 cycles.

effect was expected to be insignificant, but the mechanical twinning may be possible during fatigue loading. In order to identify the possible twinning, the Fe15Mn specimens were fatigued at 298 K and 110 K with the maximum applied stress of 750 MPa, the tests were intermittently stopped every 10,000 cycles, and the surface was observed after polishing using an optical microscope. Figure 7 shows the optical micrographs of Fe15Mn specimen fatigued at (a) 298 K/10,000 cycles (b) 298 K/20,000 cycles, (c) 110 K/10,000 cycles, and (d) 110 K/20,000 cycles. No notable number of mechanical twins were observed after fatigue loading for 10,000 cycles regardless of testing temperature. The microstructural feature did not change with further fatigue cycling to 20,000 cycles at 298 K and 110 K. Figure 8 shows the EBSD image of fatigue-failed Fe15Mn specimen at 298 K/700 MPa for 51,300 cycles. Other than the deformed structure within 50 μm from the fracture failure, no notable microstructural change, including mechanical twinning, was also observed during fatigue loading. For the formation of deformation twins, it is necessary that dislocation slip motion is relatively homogenous with length scale close to the initial grain size [30]. Therefore, the combination of high dislocation density and a large homogenous deformation length scale in the deformed low-SFE metals has been proposed to promote the initiation of mechanical twins [27]. During fatigue loading, however, the deformation is inhomogeneous since the local intense slip band is induced where the plasticity is strongly localized. For the formation of mechanical twin, a certain level of strain is believed to be applied over the massive are of specimen. Fatigue loading appears to be not sufficient to provide such a situation, and therefore, the mechanical twinning does not occur on the fatigue Fe15Mn steel specimen at ambient and cryogenic temperatures.

Figure 9 shows the SEM fractographs of Fe15Mn specimen, fatigued at (a) 298 K/600 MPa and (b) 110 K/700 MPa, and STS304L specimen, fatigued at (c) 298 K/400 MPa, and (d) 110 K/800 MPa. The fractographic analysis was made on these specimens, since each specimen showed the similar number of cycles to failure. The previous fractographic studies on high Mn steels indicated that grain boundary (GB) cracking, shown as a long shallow crack, and slip band (SB) cracking, shown as a pyramidal shaped crack, were observed on the fracture surface [43,44]. The occurrence of each mechanism was strongly dependent on the alloy composition and testing temperature [11,25,41]. Figure 9 shows that the SB cracking was relatively well developed at 298 K than at 110 K, which was particularly true for the STS304L specimen. The cleavage facets at 298 K appeared to be rougher than those at 110 K for both specimens. These morphological characteristics in fracture surface were believed to be due to the restriction in slip deformation at cryogenic temperatures. For the STS304L specimen, a considerable amount of martensite transforma-

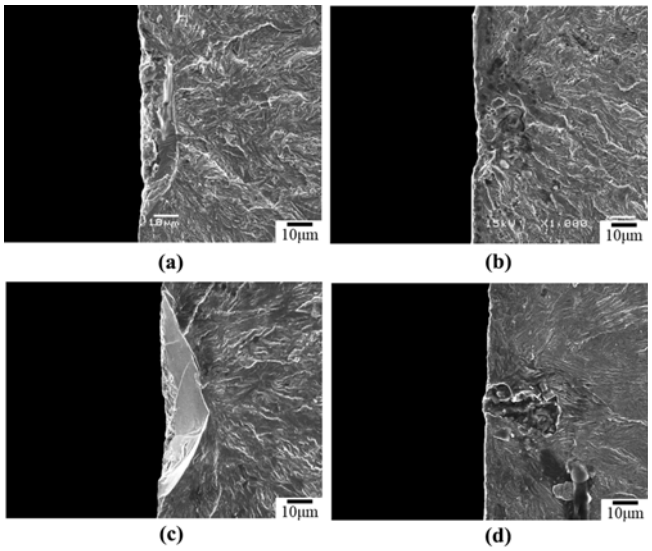

Fig. 9. The SEM fractographs of Fe15Mn specimen, fatigued at (a) 298 K/600 MPa and (b) 110 K/700 MPa, and STS304L specimen, fatigued at (c) 298 K/400 MPa, and (d) 110 K/800 MPa.

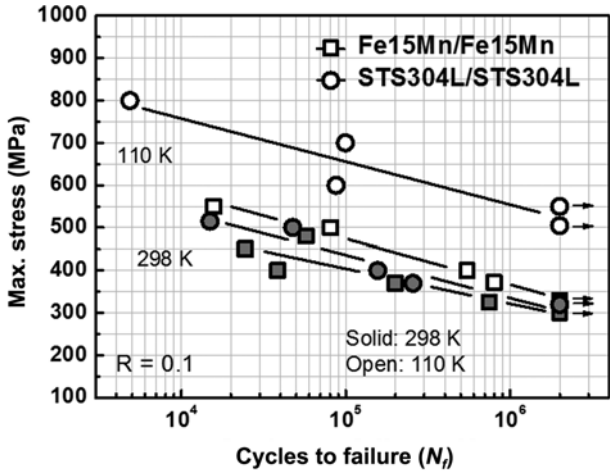

Fig. 10. The S-N fatigue curves of butt-welded joints of Fe15Mn and STS304L specimens fatigued at 298 K and 110 K.

tion occurred during fatigue loading at 110 K, and the fracture surface became very flat, typically observed for the fatigued martensite.

The uni-axial fatigue tests were also conducted on the butt-welded joints of Fe15Mn and STS304L at 298 K and 110 K, and the results are shown in Figure 10. Due to the possible microscopic imperfection associated with welding, the scatter in fatigue curves for the welded specimens was greater than that for the BM specimens, and the overall resistance to fatigue was lower for the welded specimens than the BM counterparts. Unlike the BM in Fig. 4 where the Fe15Mn specimen showed better resistance to fatigue than STS304L at 298 K, both Fe15Mn and STS304L welded specimens showed the similar resistance to S-N fatigue. With decreasing temperature from 298 K to 110 K, the welded specimens also showed the improved resistance to S-N fatigue, which was much greater for the STS304L joint than the Fe15Mn joint. Resultantly, the STS304L joint showed substantially greater resistance to S-N fatigue at 110 K. Figure 11 shows the SEM fractographs of Fe15Mn welded joints fatigued at (a) 298 K/480 MPa and (b) 110 K/500 MPa. The

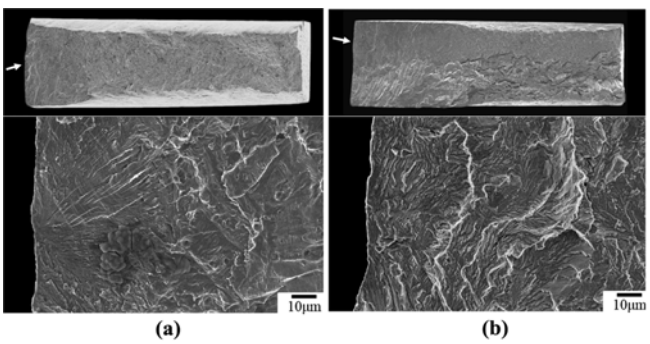

Fig. 11. The SEM fractographs of Fe15Mn welded joints fatigued at (a) 298 K/480 MPa and (b) 110 K/500 MPa.

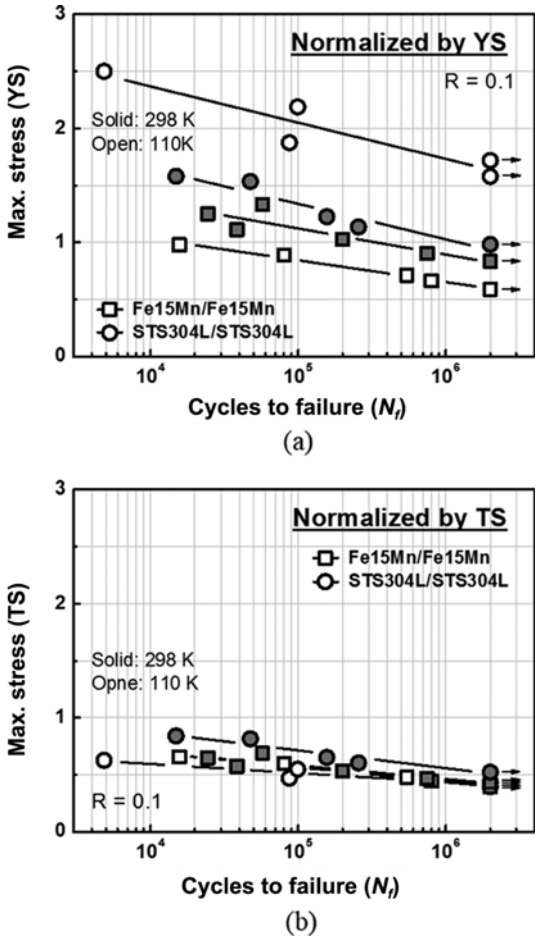

Fig. 12. The fatigue curves of Fe15Mn and STS304L welded joints at 298 K and 110 K, normalized by (a) YS and (b) TS.

crack was initiated at the corner of the specimen suggesting a sound welding. Each specimen showed the feathery appearance typical for high cycle fatigue-failure mode. As observed in the BM specimen, the facets became relatively smoother with decreasing temperature. Figure 12 shows the normalized fatigue curves of Fe15Mn and STS304L welded joints at 298 K and 110 K by (a) YS and (b) TS. Again, the S-N fatigue curves of Fe15Mn and STS304L joints at different temperatures also merged into a single line when normalized by the TS value of each specimen. The trend in Fig. 12 further confirmed that the tensile strength level largely determined the fatigue behavior of welded joints also. Figure 13 shows the hardness profile and the location of fatigue failure for the butt-welded joints of (a) Fe15Mn and (b) STS304L specimens. Both specimens showed the lowest hardness value in the fusion zone. The fatigue failure of each specimen also occurred at this fusion zone with the lowest hardness at ambient and cryogenic temperatures. The hardness-dependent fracture behavior in this figure also indicated the importance of tensile strength in determining the S-N fatigue behavior of the present welded specimens.

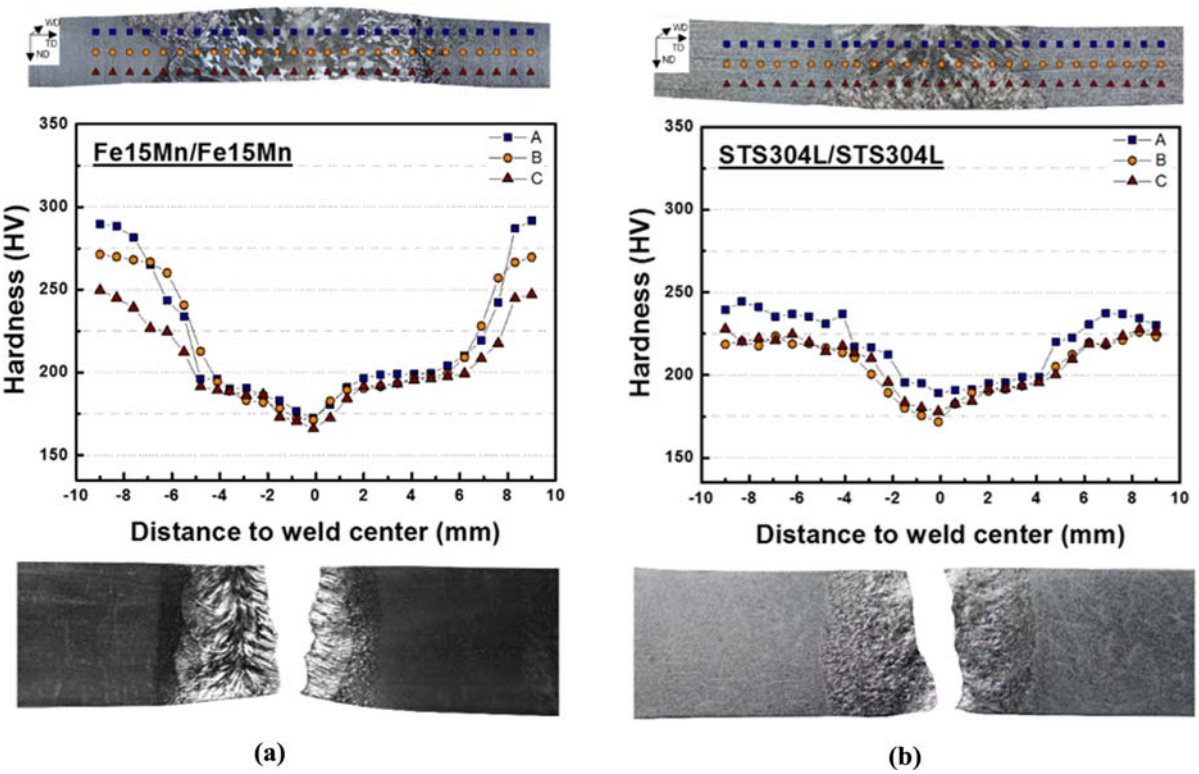

Fig. 13. The hardness profile and the location of fatigue failure for the butt-welded joints of (a) Fe15Mn and (b) STS304L specimens.

4. CONCLUSIONS

The S-N fatigue behavior of Fe15Mn austenitic steels, including base metal and butt-welded joint, was investigated at 298 K and 110 K, and the following conclusions were made.

(1) The resistance to S-N fatigue of Fe15Mn steel was greater at 298 K, while it was reversed at 110 K, than STS304L steel.

(2) Unlike the STS304L specimens which showed a substantial amount of strain-induced martensitic transformation particularly at cryogenic temperatures, the Fe15Mn specimens did not show TRIP and TWIP effects at both ambient and cryogenic temperatures.

(3) The fatigue behavior of Fe15Mn and STS304L specimens, both of which showed a considerable amount of strain hardening, was largely dependent on tensile strength at both ambient and cryogenic temperatures.

(4) The butt-welded joints of Fe15Mn and STS304L steels showed the similar trend in S-N fatigue behavior at 298 K and 110 K, which was also explained by the change in tensile strength values.

ACKNOWLEDGMENTS

This work has been supported by the Engineering Research Center (ERC) Program through the National Research Foundation of Korea (NRF) funded by the Ministry of Education, Science and Technology (2011-0030801). This work was also supported by the Technology Innovation Program (10044598, Development of the manufacturing technology for the application of high Mn alloy to the cryogenic LNG piping line) funded by the Ministry of Trade, Industry & Energy (MOTIE, Korea).

REFERENCES

1. O. Bouaziz, S. Allain, C. P. Scott, P. Cugy, and D. Barbier, *Curr. Opin. Solid State Mater. Sci.* **15**, 141 (2011).
2. D. H. Jeong, S. G. Lee, W. K. Jang, J. K. Choi, Y. J. Kim, and S. S. Kim, *Metall. Mater. Trans. A* **44A**, 4601 (2013).
3. R. Ueji, N. Tsuchida, D. Terada, N. Tsuji, Y. Tanaka, A. Takemura, and K. Kunishige, *Scr. Mater.* **59**, 963 (2008).
4. L. W. Tsay, Y. C. Chen, and S. L. I. Chan, *Int. J. Fatigue*, **23**, 103 (2001).
5. M. R. Krishnadev and R. Ghosh, *Metall. Mater. Trans. A* **10A**, 1941 (1979).
6. J. H. Baek, C. M. Kim, W. S. Kim, and Y. T. Kho, *Korean J. Met. Mater.* **7**, 579 (2001).
7. D. H. Jeong, S. G. Lee, I. S. Seo, J. Y. Yoo, and S. S. Kim, *Met. Mater. Int.* **21**, 14 (2015).
8. D. H. Jeong, S. G. Lee, I. S. Seo, J. Y. Yoo, and S. S. Kim, *Met. Mater. Int.* **21**, 22 (2015).

9. I. Karaman, H. Sehitoglu, A. J. Beaudoin, Y. I. Chumlyakov, H. J. Maier, and C. N. Tome, *Acta Mater.* **48**, 2031 (2000).
10. I. Karaman, H. Sehitoglu, K. Gall, Y. I. Chumlyakov, and H. J. Maier, *Acta Mater.* **48**, 1345 (2000).
11. S. Curtze and V. T. Kuokkala, *Acta Mater.* **58**, 5129 (2010).
12. W. C. Leslie and G. C. Rauch, *Metall. Mater. Trans. A* **9A**, 4334 (1978).
13. K. Ishida and T. Nishizawa, *Trans. Jpn. Inst. Met.* **15**, 225 (1974).
14. R. E. Schramm and R. P. Reed, *Metall. Mater. Trans. A* **6A**, 1345 (1975).
15. T. Niendorf, F. Rubitschek, H. J. Maier, J. Niendorf, H. A. Richard, and A. Frehn, *Mater. Sci. Eng. A* **527**, 2412 (2010).
16. K. T. Park, K. G. Jin, S. H. Han, S. W. Hwang, K. Y. Choi, and C. S. Lee, *Mater. Sci. Eng. A* **527**, 3651 (2010).
17. D. Canadinc, H. Sehitoglu, H. J. Maier, and Y. I. Chumlyakov, *Acta Mater.* **53**, 1831 (2005).
18. S. I. Hong and C. Laird, *Acta Metall.* **38**, 1581 (1990).
19. W. S. Owen and M. Grujicic, *Acta Mater.* **47**, 111 (1999).
20. G. Frommeyer, U. Brüx, and P. Neumann, *ISIJ Int.* **43**(3), 438 (2003).
21. A. Dumay, J.P. Chateau, S. Allain, S. Migot, and O. Bouaziz, *Mater. Sci. Eng. A* **184**, 483 (2008).
22. A. S. Hamada, L. P. Karjalainen, and M. C. Somani, *Mater. Sci. Eng. A* **467**, 114 (2007).
23. J. K. Kim, L. Chen, H. S. Kim, S. K. Kim, Y. Estrin, and B. C. de Cooman, *Metall. Mater. Trans. A* **40A**, 3147 (2009).
24. Y. S. Han and S. H. Hong, *Mater. Sci. Eng. A* **222**, 76 (1997).
25. S. Allain, J. P. Chateau, O. Bouaziz, S. Migot, and N. Guelton, *Mater. Sci. Eng. A* **387**, 158 (2004).
26. T. Niendorf, C. Lotze, D. Canadinc, A. Frehn, and H. J. Maier, *Mater. Sci. Eng. A* **499**, 518 (2009).
27. A. S. Hamada, L. P. Karjalainen, and J. Puustinen, *Mater. Sci. Eng. A* **517**, 68 (2009).
28. T. Niendorf, D. Canadinc, H. J. Maier, and I. Karaman, *Scr. Mater.* **60**, 344 (2009).
29. S. Mahajan and G. Y. Chin, *Acta Metall.* **21**, 1353 (1973).
30. E. El-Danaf, S. R. Kalidindi, and R. Doherty, *Metall. Mater. Trans. A* **30A**, 1223 (1999).
31. Z. S. Basinski and S. J. Basinski, *Acta Metall.* **33**, 1307 (1985).
32. L. P. Karjalainen, T. Taulavuori, M. Sellman, and A. Kyröläinen, *Steels Res. Int.* **79**, 404 (2008).
33. G. Baudry and A. Pineau, *Mater. Sci. Eng.* **28**, 229 (1977).
34. ASTM Standard E466, *Standard Practice for Conduction Force Controlled Constant Amplitude Axial Fatigue test of Metallic Materials*, Annual Book of ASTM Standards, **03.01** (2002).
35. ASM International Handbook Committee, *ASM Handbook 9 - Metallography and Microstructures 2004, ASM International*, **9**, 1671 (1985).
36. S. S. Kim, J. K. Kwon, Y. J. Kim, W. K. Jang, S. L. Lee, and J. K. Choi, *Met. Mater. Int.* **19**, 1 (2013).
37. D. H. Jung, J. K. Kwon, N. S. Woo, Y. J. Kim, M. Goto, and S. S. Kim, *Metall. Mater. Trans. A* **45A**, 654 (2014).
38. Z. Mei and J. W. Morris Jr., *Metall. Mater. Trans. A*, **21A** 3137 (1990).
39. J. W. Morris Jr., J. W. Chan, and Z. Mei, *Fourteenth International Cryogenic Engineering Conference and International Cryogenic Materials Conference*, p.1, Elsevier Science Inc., Kiev, Ukraine (1992).
40. F. Forouzan, A. Najafizadeh, A. Kermanpur, A. Hedayati and R. Surkialiabad, *Mater. Sci. Eng. A* **527**, 7334, (2010).
41. D. T. Pierce, J. A. Jiménez, J. Bentley, D. Raabe, C. Oskay, and J.E. Wittig, *Acta Mater.* **68**, 238 (2014).
42. A. Saeed-Akbaari, J. Imlau, U. Prahl, and W. Bleck, *Metall. Mater. Trans. A* **40A**, 3076 (2009).
43. S. S. Kim, J. K. Kwon, Y. J. Kim, W. K. Jang, S. G. Lee, and J. K. Choi, *Metall. Mater. Int.* **19**, 1 (2013).
44. J. K. Kwon, D. H. Ahn, D. H. Jeong, Y. J. Kim, N. S. Woo, and S. S. Kim, *Korean J. Met. Mater.* **52**, 757 (2014).